JOURNAL OF GEOPHYSICAL RESEARCH, VOL. 102, NO. D14, PAGES 17,209–17,217, JULY 27, 1997

Validation of atmospheric correction over the oceans

D. K. Clark,[1] H. R. Gordon,[2] K. J. Voss,[2] Y. Ge,[3] W. Broenkow,[4] and C. Trees[5]

Abstract. By validation of atmospheric correction, we mean quantification of the uncertainty expected to be associated with the retrieval of the water-leaving radiance from the measurement of the total radiance exiting the ocean-atmosphere system. This uncertainty includes that associated with the measurement or estimation of auxiliary data required for the retrieval process, for example, surface wind speed, surface atmospheric pressure, and total ozone concentration. For a definitive validation this quantification should be carried out over the full range of atmospheric types expected to be encountered. However, funding constraints require that the individual validation campaigns must be planned to address the individual components of the atmospheric correction algorithm believed to represent the greatest potential sources of error. In this paper we develop a strategy for validation of atmospheric correction over the oceans that is focused on EOS/MODIS. We also provide a description of the instrumentation and methods to be used in the implementation of the plan.

1. Introduction

Atmospheric correction of ocean color imagery in the EOS [*Asrar and Dozier*, 1994] era has been discussed in detail by *Gordon* [this issue]. Briefly, in atmospheric correction, one attempts to remove the contribution to the radiance L_t measured by the sensor that results from scattering in the atmosphere and reflection from the sea surface. If carried out correctly, the result is the water-leaving spectral radiance $L_w(\theta_v, \phi_v, \lambda)$, where θ_v and ϕ_v are the polar and azimuth angles, respectively, of a vector from the point on the ocean being examined (pixel) to the sensor, and λ is the wavelength. This is related to the upward radiance just beneath the sea surface $L_u(\theta'_v, \phi'_v, \lambda)$, where θ'_v and θ_v are related by Snell's law, and $\phi'_v = \phi_v$; that is,

$$L_w(\theta_v, \phi_v, \lambda) = \frac{T_F(\theta'_v, \theta_v)}{m^2} L_u(\theta'_v, \phi'_v, \lambda), \quad (1)$$

where m is the index of refraction of water, and T_F is the Fresnel transmittance of the air-sea interface. The time-averaged T_F as a function of wind speed W for the wind-ruffled surface has been given by *Austin* [1974]. In an attempt to remove the effects of atmospheric transmission and the solar zenith angle, *Gordon and Clark* [1981] defined the normalized water-leaving radiance $[L_w(\theta_v, \phi_v, \lambda)]_N$:

$$L_w(\theta_v, \phi_v, \lambda) = [L_w(\theta_v, \phi_v, \lambda)]_N \cos\theta_0 \cdot \exp\left[-\left(\frac{\tau_r(\lambda)}{2} + \tau_{Oz}(\lambda)\right)\left(\frac{1}{\cos\theta_0}\right)\right], \quad (2)$$

where $\tau_r(\lambda)$ and $\tau_{Oz}(\lambda)$ are the optical thicknesses of the atmosphere associated with molecular (Rayleigh) scattering and ozone absorption, respectively, and θ_0 is the solar zenith angle at the specific pixel. The exponential factor partially accounts for the attenuation of solar irradiance by the atmosphere. Ignoring bidirectional effects [*Morel and Gentili*, 1991], the normalized water-leaving radiance is approximately the radiance that would exit the ocean in the absence of the atmosphere with the sun at the zenith. This quantity is used in other algorithms to derive ocean-related properties, for example, the chlorophyll concentration. Often, it is useful to replace radiance by reflectance. The reflectance ρ associated with a radiance L is defined to be $\pi L/F_0 \cos\theta_0$, where F_0 is the extraterrestrial solar irradiance. The normalized water-leaving radiance is converted to normalized water-leaving reflectance $[\rho_w]_N$ through

$$[\rho_w]_N = \frac{\pi}{F_0}[L_w]_N. \quad (3)$$

The variation of $[\rho_w]_N$ with the phytoplankton pigment concentration C, the sum of the concentrations of chlorophyll a and its degradation product phaeophytin a, is provided by *Gordon* [this issue]. The goal of atmospheric correction of the moderate-resolution imaging spectroradiometer (MODIS) [*Salomonson et al.*, 1989], on which we focus here, is to retrieve $[\rho_w(\theta_v, \phi_v, \lambda)]_N$ at 443 nm with an uncertainty less than ± 0.002. This corresponds to an uncertainty of $\sim \pm 5\%$ at 443 nm in $[\rho_w(\theta_v, \phi_v, \lambda)]_N$ for very clear waters, for example, the Sargasso Sea in summer [*Gordon and Clark*, 1981]. In this paper we discuss the validation of the atmospheric correction procedure.

By the term validation of atmospheric correction we mean quantification of the uncertainty expected to be associated with the retrieval of $[L_w(\theta_v, \phi_v, \lambda)]_N$, or equivalently $[\rho_w(\theta_v, \phi_v, \lambda)]_N$, from the measurement of the total radiance exiting the ocean-atmosphere system. This uncertainty includes that associated with the measurement of or estimation of the ancillary data required to operate the correction algorithm, for example, surface wind speed, surface atmospheric pressure, total column ozone concentration. For a proper validation this quantification should be carried out over the full

[1]National Oceanic and Atmospheric Administration/National Environmental Satellite Data and Information Service, Camp Springs, Maryland.
[2]Department of Physics, University of Miami, Coral Gables, Florida.
[3]Research and Data Corporation, Greenbelt, Maryland.
[4]Moss Landing Marine Laboratories, San Jose State University, Moss Landing, California.
[5]CHORS, San Diego State University, San Diego, California.

Copyright 1997 by the American Geophysical Union.

Paper number 96JD03345.
0148-0227/97/96JD-03345$09.00

range of atmospheric and water types expected to be encountered in the retrievals.

2. Our Approach to Validation

Gordon [this issue] shows that in the open ocean far from the influence of land (and in the absence of the long-range transport of dust) and/or anthropogenic aerosol sources, where the atmosphere is very clear and the aerosol is located in the marine boundary layer, a simple single-scattering correction algorithm should be sufficient to provide $[\rho_w(\theta_v, \phi_v, \lambda)]_N$ with the desired accuracy at 443 nm. For more turbid atmospheres, in which multiple scattering is important, *Gordon and Wang* [1994a] developed an algorithm that uses a set of candidate aerosol models developed by *Shettle and Fenn* [1979] to assess the effects of multiple scattering. This algorithm performs well as long as the absorption properties of the candidate aerosol models are similar to the actual aerosol present in the atmosphere. Furthermore, if the aerosol is nonabsorbing or weakly absorbing, the algorithm is insensitive to the vertical distribution of the aerosol. However, difficulties with this algorithm can occur under certain conditions, one of which is when the aerosol is strongly absorbing. In this case, the successful operation of the algorithm still requires that the candidate aerosol models be representative of the actual aerosol present and, in addition, that the thickness of the layer in which the dominant aerosol resides must be known or estimated with an accuracy of $\sim\pm 1$ km.

On the basis of these observations it is reasonable to focus the atmospheric correction validation on regions dominated by (1) a locally generated maritime aerosol and (2) strongly absorbing aerosols. In this manner it is possible to establish an uncertainty estimate characteristic of regions for which the atmospheric correction should be excellent (and applicable to much of the world's oceans) and to estimate how the uncertainty increases in regions with aerosols that present correction problems.

The open ocean, free of land and anthropogenic sources, represents the most favorable of conditions for atmospheric correction. In such a region the aerosol is locally generated and resides in the marine boundary layer. In the absence of intense stratospheric aerosol, as might be present after a volcanic eruption, and in the absence of thin cirrus clouds, only whitecaps and residual Sun glitter need to be removed in order that conditions satisfy those assumed in the development of the correction algorithm, i.e., a relatively clear two-layer atmosphere with aerosols in the lower layer. Under such conditions the error in the water-leaving radiance due to the aerosol removal should be small and specifying this component of the error field under these conditions relatively simple. When the error due to the aerosol is small, errors due to whitecaps and Sun glitter may make a significant contribution to the overall error, therefore a location with the conditions described above would be ideal for specifying the error fields due to these processes. The site chosen for such validation is in the waters off Hawaii.

There are two common situations with strongly absorbing aerosols in which the atmospheric correction algorithm may not retrieve the water-leaving radiances within acceptable error limits: situations in which the aerosol absorption is relatively independent of wavelength (urban aerosols transported over the oceans) and situations in which the aerosol absorption has significant spectral dependence (desert dust transported over the oceans). Clearly, it is important to perform validation in regions and times where significant amounts of both types of absorbing aerosol are expected to be present over the water. In the case of urban pollution our chosen location is the Middle-Atlantic Bight during summer (excellent logistics as well). For desert dust there are two important regions: the North Pacific (Gobi Desert influence) and the tropical North Atlantic (Saharan Desert influence). We plan a validation cruise in the tropical North Atlantic; Japanese colleagues will concentrate on the North Pacific.

In order to utilize imagery in the more turbid case 2 waters near coasts, it is critical to understand the limitations that significantly higher (than typical oceanic) concentrations of suspended particulate matter in the water place on atmospheric correction. Thus validation of atmospheric correction should also be carried out in a coastal region of spatially varying turbidity. Such a validation can be effected in the Middle-Atlantic Bight by making measurements at a set of stations successively closer to the coast. In this manner it will be possible to combine the validation cruises for studying the limitations imposed by urban aerosols and by waters of moderate turbidity.

All ocean color sensors exhibit problems that can be traced to their particular design. For MODIS, which uses linear array detectors in a push broom configuration, internally scattered stray light from bright targets can contaminate the radiometric measurement of L_t. Thus it is important to examine the influence of stray light on atmospheric correction. For example, how close can one perform adequate atmospheric correction to a cloud bank or coastline? Such examination can be effected by studying the atmospheric correction in broken cloud fields and near islands in clear water. The Hawaii optical mooring site (section 4.2) appears to be ideal for such studies and would provide error bounds on normalized water-leaving radiances under such conditions. This single site should be adequate for assessing this component of the error field.

Validation of any algorithm developed for removal of stratospheric aerosols and/or thin cirrus clouds is also required; however, it will not be necessary to conduct a focused validation experiment for this purpose. One need only track the quality of the atmospheric correction in the experiments recommended above with regard to the scene reflectance at 1380 nm (used to indicate the presence and amount of stratospheric aerosol and/or thin cirrus [*Gao et al.*, 1993; *Gordon et al.*, 1997]) to assess the efficacy of this component of the algorithm.

Finally, an important component of validation is an estimate of the day-to-day consistency and the long-term stability of the retrieved radiances. The Hawaii optical mooring site (section 4.2) will provide the water-leaving radiances required to monitor the quality of the retrievals on a continual basis.

3. Required Measurements

The radiance $L_t(\lambda)$ measured at a wavelength λ by a spaceborne sensor can be decomposed as follows:

$$L_t(\lambda) = L_r(\lambda) + L_a(\lambda) + L_{ra}(\lambda) + tL_w(\lambda), \qquad (4)$$

where L_r is the radiance resulting from multiple scattering by air molecules (Rayleigh scattering) in the absence of aerosols, L_a is the radiance resulting from multiple scattering by aerosols in the absence of the air, L_{ra} is the interaction term

between molecular and aerosol scattering [*Deschamps et al.*, 1983], L_{wc} is the contribution to the radiance from whitecaps, and L_w is the desired water-leaving radiance. The term L_{ra} accounts for the interaction between Rayleigh and aerosol scattering, e.g., photons first scattered by the air then scattered by aerosols, or photons first scattered by aerosols then air. The contribution from specular reflection of the solar beam from the sea surface (Sun glitter) is ignored, as the algorithm is not valid close to the glitter pattern, so validation will not be attempted there. However, the contribution from sky radiance specularly reflected from the sea surface is included in L_t. In this equation, t is the diffuse transmittance of the atmosphere.

The goal of atmospheric correction is the retrieval of L_w from L_t in (4) and the subsequent estimation of $[L_w(\lambda)]_N$. Obviously, to validate the atmospheric correction, it is necessary to compare near-simultaneous satellite-derived and surface-measured values of the retrieved quantity: $[L_w]_N$ (or $[\rho_w]_N$). Typically, in situ measurements of $L_u(\theta'_v, \phi'_v, \lambda)$ are obtained only for $\theta'_v = 0$, and $[L_w]_N$ is derived for this direction and used to develop algorithms for relating the water-leaving radiance to ocean properties. It has usually been assumed that $L_u(\theta'_v, \phi'_v, \lambda)$ is nearly independent of θ'_v and ϕ'_v. However, recently, Morel and coworkers [*Morel and Gentili*, 1991, 1993; *Morel et al.*, 1995] have shown that L_u varies considerably, depending on θ'_v, ϕ'_v, θ_0, and ϕ_0, where ϕ_0 is the solar azimuth. Thus for purposes of validation, one must measure $L_u(\theta'_v, \phi'_v, \lambda)$, i.e., the upwelling spectral radiance just beneath the sea surface in the direction that the sensor is viewing. L_w is then determined with (1). As MODIS views the ocean with a spatial resolution of ~1 km at nadir, an assessment of the variability of $L_u(\theta'_v, \phi'_v, \lambda)$ within the pixel under examination must also be carried out to obtain a pixel-averaged $L_u(\theta'_v, \phi'_v, \lambda)$. This can be effected by mapping the phytoplankton pigment concentration [*Gordon et al.*, 1980] in the vicinity of the biooptical ship station and using a radiance model (e.g., *Gordon and Clark* [1981] or *Gordon et al.* [1988]) relating it to $[L_w(\lambda)]_N$.

In principal, this is all that is required to assess the error limits for $[L_w(\lambda)]_N$ or $[\rho_w(\lambda)]_N$. However, it provides little or no understanding as to the cause of the error, for example, an incorrect choice of the aerosol model from a collection of candidates, an incorrect vertical distribution assumed for the aerosol, etc. For a complete assessment it will be important to understand what part of the atmospheric correction algorithm is at fault. Furthermore, such an understanding will facilitate algorithm "fine tuning," for example, a modification of a correction procedure in the algorithm, a modification in the candidate aerosol models, a modification in the vertical distribution, etc. This requires what we term "auxiliary" measurements, i.e., measurements of quantities other than that which is being validated. Several such measurements are discussed next.

Since the major (highly variable) component to be removed during atmospheric correction is the aerosol, it is important to make detailed measurements of the columnar aerosol optical properties as part of the validation effort. Quantities to be measured include the spectral aerosol optical thickness $\tau_a(\lambda)$ and the spectral sky radiance $L_{\text{Sky}}(\lambda)$, both close to (the aureole) and far from the Sun. From such measurements it is possible to obtain the columnar aerosol size distribution, aerosol phase function, and aerosol single-scattering albedo, an index of the aerosol absorption [*Gordon and Zhang*, 1996; *Kaufman et al.*, 1994; *King et al.*, 1978; *King and Herman*, 1979; *Nakajima et al.*, 1983; *Wang and Gordon*, 1993]. These data will be used to determine the applicability of the aerosol model selected by the algorithm for use in the atmospheric correction and to provide a determination of the presence or absence of strongly absorbing aerosols. The latter is critical, as it is known that the algorithm does not perform well in the presence of strongly absorbing aerosols.

Table 1. Measurements and Associated Quantities They Help Determine or Understand

Measurement	Determines or Contributes to Understanding
$L_u(\lambda)$ at nadir	$L_w(\lambda)$
$L_u(\theta'_v, \phi'_v, \lambda)$	$L_w(\lambda)$
$C(x, y)$	$L_w(\lambda, x, y)$
$L_{\text{Sky}}(\lambda)$	$L_a(\lambda) + L_{ra}(\lambda), t$
$\tau_a(\lambda)$	$L_a(\lambda) + L_{ra}(\lambda), t$
Lidar	$L_a(\lambda) + L_{ra}(\lambda)$
Whitecaps	$L_{wc}(\lambda)$
P_0, $\vec{W}$	L_r

As mentioned in section 2, the correction algorithm is insensitive to the vertical distribution of the aerosol only if it is weakly absorbing or nonabsorbing: a degradation in the accuracy of the retrieved water-leaving radiances is expected in the presence of significant quantities of absorbing aerosol in the free troposphere. Because of this it is important to be able to assess the vertical structure of the aerosol. The most direct technique of effecting this is lidar [*Sasano and Browell*, 1989; *Spinhirne*, 1993]. We plan to operate a shipborne lidar during our validation campaigns.

Whitecaps on the sea surface can also result in larger-than-required uncertainty in $[\rho_w(\theta_v, \phi_v, \lambda)]_N$ [*Gordon and Wang*, 1994b; *Koepke*, 1984], unless the increase in the spectral reflectance of the ocean-atmosphere system can be estimated within about ±0.002. The severity of the whitecap perturbation depends on the spectral form of the reflectance [*Frouin et al.*, 1996; *Gordon*, this issue; *Schwindling*, 1995]. Thus an estimate of the whitecap contribution to the perturbation of the $[\rho_w(\theta_v, \phi_v, \lambda)]_N$ is required.

Finally, the ancillary data required to operate the atmospheric correction algorithm and, in the processing of MODIS data estimated from numerical weather models, must also be measured. These include surface atmospheric pressure, wind speed, and wind direction.

These measurements, which we believe are required to provide a complete data set for understanding the uncertainties associated with atmospheric correction, are summarized in Table 1. In the table and henceforth, we refer to ship-based campaigns during which such measurements are carried out as a Marine Optical Characterization Experiment (MOCE).

4. Instrumentation and Measurements

The main validation effort, as envisaged, will be carried out via ship-based and buoy-based measurements. The ship-based validation will involve the more complete set of measurements, because much of the instrumentation cannot be operated from buoys. We shall discuss each in detail.

4.1. Ship-Based Instrumentation

A complete set of measurements for validation of atmospheric correction must be ship-based, as the most fundamen-

tal measurement $L_u(\theta'_v, \phi'_v, \lambda)$ can only be made from such platforms. The basic measurements to be carried out at sea are high spectral resolution (~3–4 nm) measurements of L_u at nadir ($\theta'_v = 0$, actually $\theta'_v < 5°$), measurement of $L_u(\theta'_v, \phi'_v, \lambda)$ in a few spectral bands (full width at half maximum (FWHM) ~10 nm), measurement of the augmentation of the water-leaving reflectance by whitecaps, measurement of the aerosol optical thickness (FWHM ~4 nm) and sky radiance (FWHM ~10 nm) in a few spectral bands, and measurement of ancillary parameters such as surface wind speed and direction and atmospheric pressure at the surface. Instrumentation developed to meet these measurement requirements is described next. Protocols for most of the measurements are provided by *Mueller and Austin* [1992, 1995].

4.1.1. Upwelling spectral radiance at nadir. Typically, for remote sensing applications the optical measurements are performed in the near-surface waters at three or four depths z. The selection of these depths depends on the clarity of the water. The optical instrument which measures upwelled spectral radiances $L_u(z, \lambda)$ and downwelled spectral irradiance $E_d(z, \lambda)$ is suspended from a buoy and drifted away from the ship in order to avoid shadowing by the ship. Onboard the ship, a second spectrometer measures the downwelling sky and Sun spectral irradiance just above the sea surface $E_s(z, \lambda)$ when the submersed spectrometer is at depth z in order to normalize for the variations in the incident irradiance. The shallowest observations of upwelled spectral radiances (nominally 1 m) are then propagated upward to just beneath the sea surface by first calculating the upwelled spectral radiance attenuation coefficient $K_L(\lambda)$ using

$$K_L(\lambda) = \frac{1}{z_2 - z_1} \ln \left[\frac{L_u(z_1, \lambda)}{E_s(z_1, \lambda)} \frac{E_s(z_2, \lambda)}{L_u(z_2, \lambda)} \right], \quad (5)$$

where z_1 and z_2 are the two shallowest depths at which measurements are carried out ($z_1 < z_2$). Then the radiance loss between the surface and z is accounted for through

$$L_u(0, \lambda) = L_u(z_1, \lambda) \exp [K_L(\lambda) z_1]. \quad (6)$$

The subsurface upwelled radiances are then transmitted through the sea surface using (1) and normalized with (2). These high-resolution spectra are then convolved with the satellite sensor's spectral response, $S_i(\lambda)$ for band i, to form the band-averaged water-leaving radiance [*Gordon*, 1995]:

$$\langle [L_w(\lambda)]_N \rangle_i = \int S_i(\lambda) [L_w(\lambda)]_N \, d\lambda. \quad (7)$$

Examples of spectra of $L_u(z, \lambda)$ derived from similar measurements can be found in the work of *Clark et al.* [1980].

Since effective application of ocean color satellite observations, to derive biooptical products, rely totally on retrieving accurate and precise water-leaving radiances, a new marine optical instrumentation and a buoy system to enhance its in situ measurement capability has been developed. A prototype marine optical system (MOS) has been constructed and tested. The operational version of this system is now in its final construction phase and is scheduled for at-sea test and evaluation during the summer 1996. The system uses a modular design concept which has provided a high degree of flexibility and has facilitated the ease in which instrument upgrades can be implemented. The concept was constrained by the buoy requirement that necessitated the instrument be capable of maintaining measurement integrity while being unattended for long periods of time. This constraint has led to a design which minimizes the number of moving parts (one) and has resulted in the spectrographic application of concave holographic diffraction gratings. These spectrograph gratings approximate a flat focal field to the degree that planar silicone photodiode arrays may be used as detectors. Inherent within this technology are the features of simplicity, compactness, durability, and stable high-performance system characteristics. The new operational version uses a convex holographic grating spectrograph with a cooled CCD detector system. These modifications are being implemented in order to improve image quality, dynamic range, and signal to noise ratios. Additionally, the shipboard system is being modified to utilize fiber optics to avoid the instrument self-shadowing errors as described by *Gordon and Ding* [1992]. This is particularly important in turbid waters or in the red and near-infrared regions of the spectrum.

Laboratory radiometric calibrations of the MOS are performed prior to and after each deployment. Spectral standards for irradiance are either National Institute of Standards and Technology (NIST) traceable or NIST standard lamps (1000 W FEL'S). NIST protocols for irradiance calibrations are used in conjunction with commercial systems (EG&G GAMMA Scientific model 5000 and Optronics model 420) which have integrating spheres for radiance calibrations. We believe that this instrument is capable of measuring in-water radiance under ideal conditions with an uncertainty of ~2%. During the laboratory calibrations, portable reference lamps are measured and then utilized during the at-sea deployments to provide a time history of the system response stability. To insure consistency between these calibrations and calibration scales used by others, we participate in the SeaWiFS Intercalibration Round-Robin Experiments (SIRREX) [*Johnson et al.*, 1996; *Mueller*, 1993; *Mueller et al.*, 1994, 1996]. For the buoy application a submersible reference lamp has been developed for divers to perform monthly checks of the system's stability. These are sufficiently stable to detect a change in the system response of ~2%. Wavelength calibrations are performed with five low-pressure lamps, which provide numerous emission lines over the instrument's spectral range; however, with the modifications mentioned above, solar Fraunhofer lines can be used for wavelength calibration.

4.1.2. Upwelling spectral radiance distribution. The spectral upwelling radiance distribution $L_u(z, \theta'_v, \phi'_v, \lambda)$ will be measured using a radiance distribution camera system (RADS) [*Voss*, 1989; *Voss and Chapin*, 1992]. This system employs a fish-eye camera lens to image the upwelling radiance distribution onto a thermoelectrically cooled CCD camera (First Magnitude, Starscape IIb). Included in the optical path are interference filters which are used to select the spectral region of interest. There are four possible filter positions on each of two filter wheels which can be used to obtain the upwelling radiance distribution in six different spectral bands. Since only the near-surface radiance distribution is needed in this application, the instrument will be deployed by suspending it beneath a float at the depth z_L of 1.5–2 m. This will allow the instrument to drift away from the ship and avoid ship shadow contamination of the data [*Gordon*, 1985]. Data reduction and instrument calibration are performed using standard procedures which have been described elsewhere [*Voss and Zibordi*, 1989]. Although absolute radiometric calibration is not so good as for MOS, the relative response of the instrument as a function of θ_v is known with an uncertainty of ~2%; therefore by

normalizing to the near-nadir MOS measurement, it should be possible to measure $L_u(z_L, \theta'_v, \phi'_v, \lambda)$ with an uncertainty $\lesssim$2.5%. $L_u(z_L, \theta'_v, \phi'_v, \lambda)$ will be propagated to the surface using K_L derived from the near-nadir-viewing MOS (section 4.1.1). This is acceptable as $L_u(z, \theta'_v, \phi'_v, \lambda)$ decays with depth in a manner that is a weak function of θ'_v and ϕ'_v. If necessary, the radiance distribution will be interpolated between spectral bands using the L_u near-nadir spectrum discussed in the last paragraph.

To estimate $[L_w(\theta_v, \phi_v, \lambda)]_N$, it is necessary to propagate $L_u(z, \theta'_v, \phi'_v, \lambda)$ to the surface and then through the air-sea interface. In clear water, propagation to the surface is essentially error free, as K_L is very small in the blue-green spectral region. Propagation across the interface poses no problem when the surface is flat; however, at wind speeds of a few meters per second, propagation across the interface will lead to additional error in T_F. We believe the largest source of error in $[L_w(\theta_v, \phi_v, \lambda)]_N$ will be environmental noise induced by the moving sea surface, which results in fluctuations in the marine light field. These are unavoidable and their effects can only be estimated on a case-by-case basis. In their absence it should be possible to measure $[L_w(\theta_v, \phi_v, \lambda)]_N$ with sufficient accuracy in the blue to determine if MODIS meets the stated goal: a 5% uncertainty in the retrieved $[L_w]_N$ in very clear water in the blue.

4.1.3. Whitecap reflectance contribution. To determine the whitecap contribution to the top-of-the-atmosphere reflectance, a new radiometer system has been constructed [*Moore et al.*, 1996]. This instrument system consists of a narrow field-of-view radiometer, video camera system, downwelling irradiance sensor, wind speed and direction instruments, and a Global Positioning System (GPS) receiver. The radiometer and irradiance sensor have six spectral bands each, with matching filters to enable the upwelling reflectance of the sea surface to be calculated. The radiometer and video camera system are aligned to view the same scene and deployed 5–10 m in front of the bow of the ship to obtain a downward view of the surface uncontaminated by ship wake effects even while the ship is under way. The full angle field of view of the radiometer is approximately 1°, so the diameter of the surface sampling area is typically 20 cm (depending on the height of the bow above the sea surface). The video camera signal is recorded and the images are time stamped to allow synchronization of the video images and radiometer data. The video images are useful for identifying whitecaps and other surface features in the data stream, for example, Sun glitter. The data from the radiometer, irradiance sensor, and wind speed and direction instrument are digitized at 1000 Hz, and the average of 100 samples are recorded at 0.5 Hz along with the GPS position. By continuously measuring the total reflectance of the ocean surface, the whitecap contribution to the signal may be determined. Samples in the data stream, with and without whitecaps, can be found, and therefore the augmentation of the reflectance by whitecaps can be determined. Since the relative wind speed, direction, and ship heading and speed are also recorded, the relationship between the true wind speed and whitecap augmentation of the reflectance can be studied. Such a relationship is a required ingredient in the whitecap correction algorithm [*Gordon*, this issue].

4.1.4. Aerosol optical thickness. The aerosol optical thickness is measured using a standard Sun photometer [*d'Almeida et al.*, 1983]. The total optical depth is determined in spectral bands which do not have sharp molecular absorption bands. In this manner the only other components, besides aerosols, which have significant contributions are the molecular (Rayleigh) scattering and the broad Chappuis absorption band of ozone. Thus when the total optical thickness is determined, the aerosol optical thickness can be found by subtraction of the Rayleigh optical thickness, determined by calculation [*Young*, 1980], and the ozone optical thickness, determined by ozone climatologies [*Klenk et al.*, 1983], or by direct measurement, and knowledge of the wavelength dependence of ozone absorption [*Nicolet*, 1981; *Vigroux*, 1953].

4.1.5. Sky radiance. On land, an automatic pointing instrument, for example, the automatic Sun and sky radiometer (ASSR) [*Holben et al.*, 1997] may be used to make sky radiance distribution measurements, but on a ship, obtaining a stable reference is difficult and expensive. Thus for our shipborne program we will use a camera system similar to the RADS system described above. This fish-eye camera system is mounted in a "stable table" which is an active servocontrolled table to maintain an approximate vertical reference. Otherwise the overall system is very similar to the in-water system. The sky camera has also been equipped with polarizers to enable measurement of the first three elements of the Stokes vector in the sky radiance distribution (the linear polarization components) [*Liu*, 1996].

Because of the rapid change in sky radiance near the Sun, the RADS system requires that a 10° portion of the sky around the Sun be blocked to prevent flare in the camera lens system. To acquire the sky radiance near the Sun, an important component in assessing the aerosol absorption [*Gordon and Zhang*, 1996], another instrument has been constructed. This instrument, a solar aureole camera system, is designed to measure the sky radiance for the region from 2° to 10° from the solar disk. This instrument is based on a cooled CCD camera system (Spectra source, MCD1000). In this system a 35 mm camera lens (50 mm focal length) is used to image the sky around the Sun. An interference filter is attached to the front of the lens to select the spectral region of interest, and a small aperture (1 cm) is placed in front of the interference filter. A small occulting disk is placed approximately a meter in front of the camera and is oriented such that the shadow of this disk falls over the aperture on the interference filter. Thus the direct solar image is blocked from the camera system, yet the area around the Sun can be imaged. The system is controlled, via software, to be operated with a push button on the camera itself. When the shadow of the occulter is in the correct position, the operator triggers the push button which tells the camera system to operate the shutter and obtain an image. Immediately afterward, a dark image is obtained to be used in the data reduction process. Calibration of this system is similar to the RADS system. The calibration procedures required include camera system roll-off and flat fielding, system linearity, absolute radiance calibration, and spectral calibration. These procedures have been performed as described by *Voss and Zibordi* [1989].

4.1.6. Phytoplankton pigments. Normally, the measurement of the phytoplankton pigment concentration, C, is not used in this type of validation process. However, for the very clear water cases ($C \lesssim 0.25$ mg/m^3) the water-leaving radiance spectral variance can be estimated as a function of pigment concentration [*Gordon and Clark*, 1981]. Thus measurement of C as a function of position (x, y) near a primary biooptical station allows an estimation of the spatial variability of L_w. This can be accomplished by a grid of ship tracks traversed while continuously measuring chlorophyll *a* fluores-

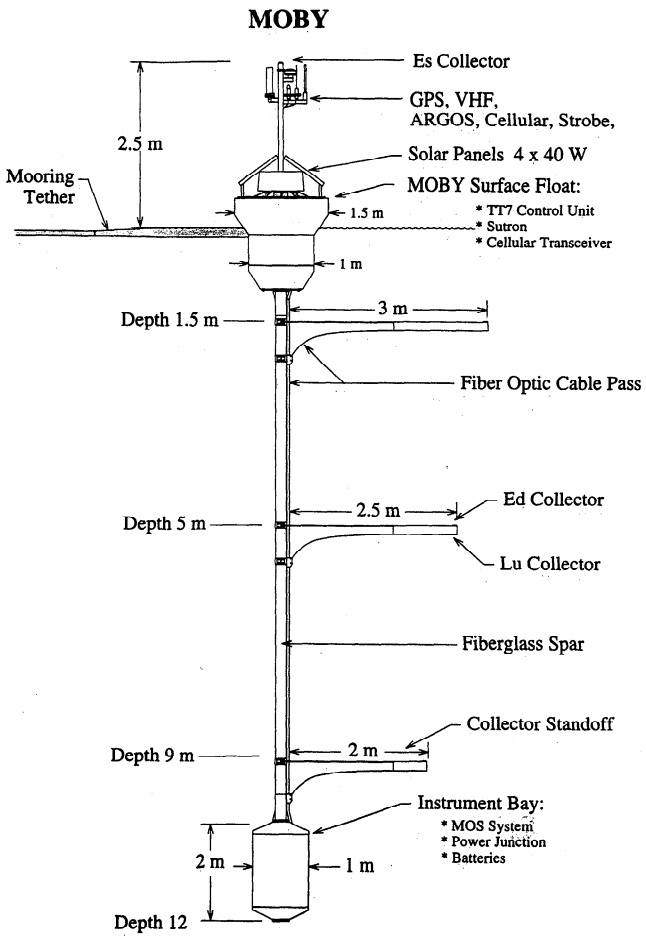

Figure 1. Schematic of the marine optical buoy system (MOBY II).

cence. A fluorometer, depth sensor, and water-pumping system are towed while the ship is under way at near-surface depth (5 m typically). Calibration of the fluorometric signal is conducted from high-frequency sampling (every 15 min) of the water pumped from the towed depth for laboratory extraction of pigments. Contour maps of the pigment distribution and the estimated normalized water-leaving radiances are then generated for satellite intrapixel variability analyses.

4.1.7. Ancillary measurements. Apparent wind speed and direction are determined using a standard instrument manufactured by Young Co. (model 05103). The apparent wind observations are corrected for the ship's heading and speed from the ship's navigation instrumentation (gyro and speed log). Relative humidity and air temperature are measured with Vaisalla sensor systems (models HMD 30/UB/YB and HMD/W 30YB, respectively). Atmospheric pressure is obtained from a digital pressure transducer manufactured by Setra (model 470). These measurements are all continuously logged at 1 Hz along with GPS time and position. The data are then processed into mean values at specified time intervals, i.e., mean atmospheric pressure every 4 hours. Ozone concentrations may be obtained from various sources. For the MOBY site (section 4.2, Figure 2), column ozone can be obtained from the National Oceanic and Atmospheric Administration/Climate Monitoring and Diagnostics Laboratory (NOAA/CMDL) site at Mauna Loa (G. Koenig, personal communication, NOAA/CMDL, 1996). For other sites in the northern hemisphere, data can be obtained from the WMO Ozone Mapping Centre (http://www.athena.auth.gr:80/ozonemaps/) which derives the data from SBUV-2 satellite data and ozone sondes around the world. These data will be used to assess the efficacy of the ancillary data products used in the correction algorithm [*Gordon*, this issue].

4.2. Buoy-Based Instrumentation

The marine optical buoy system (MOBY), illustrated in Figure 1, is tethered to a slack-line moored main buoy. MOBY is a 15 m, 2500 lb, wave-rider buoy which emulates an "optical bench" with a 12 m column extending into the sea. The surface buoy floatation (manufactured by Moorings System Inc.) is 1.7 m in diameter, with four 40-W solar panels mounted to the antenna support column. The surface buoy houses the controlling computers, data storage, electronics, cellular modem, and computer battery. The MOS, discussed in section 4.1.1, has been reconfigured for the buoy application. The instrument along with four 200 A/h gel cell marine batteries is located in the subsurface housing at the bottom of the buoy. The apparent optical properties (upwelled radiances and downwelled irradiances) are measured by a series of remote collectors positioned on arms extending away from the central column. The arms may be positioned at varying depths, typically 1.5, 6, and 10 m, along the column. The E_s sensor is located at the top of the surface buoy. The remote collectors are coupled to 1 mm, multimode fiber-optic cables which are terminated at a fiber-optic rotary selector (multiplexer). This optical multiplexer is mounted to one of the MOS entrance windows. Multiplexer ports are selected, and the energy incident on the remote collector relays the light into the MOS optical train and detectors. The optical and ancillary data are relayed to the surface computer and stored on disk for future access via a cellular telephone link. The transmitted data will be converted into calibrated radiances and a water-leaving radiance database developed. This will be used for validation as well as for sensor quality control monitoring and algorithm development.

The selection of the site for MOBY was primarily based on the clear-water water-leaving radiance criterion [*Gordon and Clark*, 1981], logistics, and survivability. The site selected is located at 20°49.0′N and 157°11.5′W in 1200 m of water and is approximately 10 nautical miles from the west coast of the Hawaiian Island of Lanai (Figure 2). The mountains on the Islands of Molokai, Lanai, and Maui provide a lee from the dominant trade winds (note mean wind speed isopleths in Figure 2). This lee reduces the amount of sea, swell, and cloud cover at the mooring site which increases the probability of mooring survivability and cloud free satellite coverage. Logistics are conducted from a dockside operational support facility which has been constructed at the University of Hawaii's Marine Operations Facility in Honolulu. GTE-MobleNet has excellent cellular coverage in the region, facilitating the transfer of relatively large MOBY observational data sets back to the MOBY support facility computer or to the mainland. University of Hawaii ships are utilized for MOBY deployments and maintenance. The transit time to the MOBY site from Honolulu is approximately 6 hours, allowing for a relatively quick response time in case emergency service is required.

In support of the MOBY effort, a land-based automatic Sun and sky radiometer [*Holben et al.*, 1996] (ASSR, CIMEL Electronique) has been installed at a remote site on the west coast of Lanai at 20°49.57′N, 156°59.1′W (Figure 2). The ASSR measures the direct solar irradiance in several wavelength

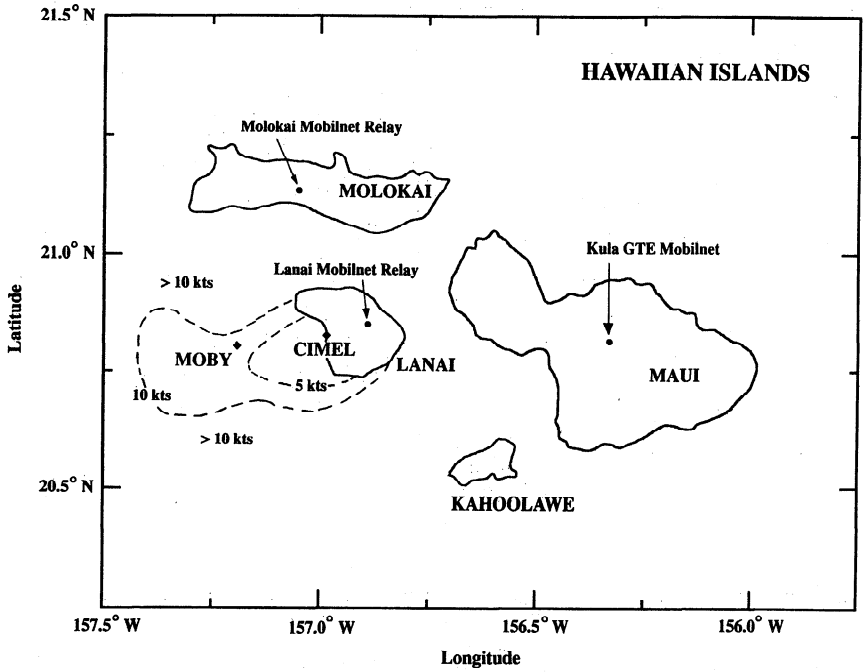

Figure 2. Chart of the calibration/validation site occupied by MOBY, along with isopleths of mean wind speed in the vicinity of the site. Also shown are the ASSR site and the MobilNet relay sites.

bands (440, 670, 870, 937, 940, and 1020 nm) in the visible every 15 min during the morning and afternoon. In addition, the instrument measures the sky radiance in the principal plane (the Sun-zenith plane) and along the almucantar (the collection of azimuthal angles with the same zenith angle as the Sun) in several wave bands (440, 670, 860, and 1020 nm) 3 times each morning and afternoon. These data are collected automatically and are sent via the GOES satellite to NASA Goddard where it can be accessed over the Internet. In its location on Lanai it has an unobstructed view to the south and west for measurement of the sky radiance and the aerosol optical thickness. Volcanic activity on the Island of Hawaii, which lies approximately 165 miles to the southeast of the site, will produce unique aerosol occurrences when the surface winds are from the southeast. The frequency of these wind conditions is approximately 10 days per year (J. Porter, University of Hawaii, personal communication, 1996). The observations are acquired approximately 11.3 nautical miles from the MOBY site and should be representative of the atmospheric conditions in that region. Shipboard atmospheric measurements will be made for comparison purposes on the MOBY quarterly maintenance cycles. In Figure 3 a schematic is provided which summarizes the measurements to be carried out during MOCE and MOBY validation exercises.

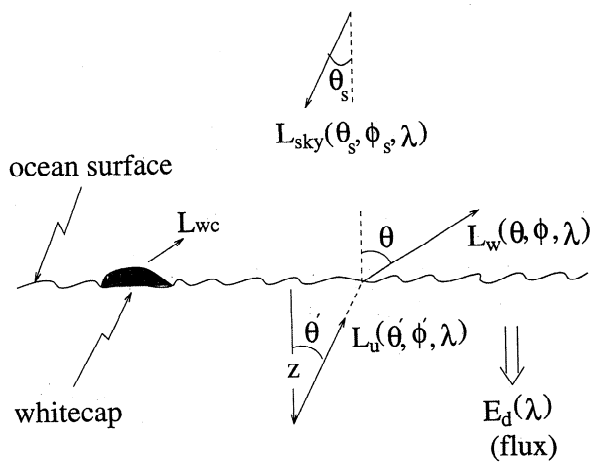

MEASUREMENTS

Ship (MOCE)	Buoy (MOBY)
$L_u(0,\phi',\lambda)$, $E_d(\lambda)$, 3 Depths	$L_u(0,\phi',\lambda)$, $E_d(\lambda)$, 3 Depths
$L_u(\theta',\phi',\lambda)$, 1 Depth	—
$\tau_a(\lambda)$ (Sun Photometer)	$\tau_a(\lambda)$ (ASSR)
$L_{Sky}(\theta_s,\phi_s,\lambda)$ (Sky Camera)	$L_{Sky}(\theta_s,\phi_s,\lambda)$ (ASSR)
$L_{wc}(\lambda)$, $\vec{W}$ (Whitecap Rad.)	$\vec{W}$
Solar Aureole (Aureole Camera)	Solar Aureole (ASSR)
$C(x,y)$ (Fluorometric)	—
LIDAR (Ship)	LIDAR (Mauna Loa)
P_0, Ozone	P_0, Ozone

Figure 3. Summary of the Marine Optical Characterization Experiment and MOBY measurements.

5. Other Sources of Validation Data

A flaw in the validation approach described in the previous sections is the sparseness of the number of simultaneous surface-satellite collection events expected. To increase both the number of collection events and the scale over which the validation is effected, we envisage the use of two additional data sources: (1) fluoromentrically determined pigment concentration (C) along the surface tracks of "ships of opportunity" and (2) $L_w(\lambda)$ estimated from $L_u(\lambda)$ measurements obtained from free-drifting sensors floating at the sea surface. Along ship tracks, C measurements can be converted to a low-accuracy estimate of $[L_w(\lambda)]_N$ using the radiance model of *Gordon et al.* [1988]. Although the free-drifting sensor measurement provides the desired $L_w(\lambda)$ directly, the accuracy is

Table 2. Overview of Validation Measurements

Platform	Radiometric Accuracy	Ancillary Data	Sampling Scale: Temporal (Samples/Year)	Sampling Scale: Spatial
Ship (MOCE)	very high	very high	15–20	small
Buoy (MOBY)	high (nadir)	very high	75–100	point
Ship ($C \rightarrow L_w$)	low (model)	high	contemporaneous	mesolarge
Drifters	low (fouling)	satisfactory	many	meso

poorly defined because of biofouling problems. Despite these flaws, both approaches can provide a significant increase in the quantity of validation data available. Combining the lower-accuracy, higher-frequency data from these sources with the higher-accuracy, lower-frequency data from MOCE and MOBY campaigns will greatly expand the scope of validation. This is summarized in Table 2.

6. Concluding Remarks

We have described the requirements for validating the MODIS atmospheric correction algorithm over the oceans and presented a plan for effecting the validation. The description and plan are applicable to validation of other ocean color sensors as well, as long as account is taken of any particular sensor peculiarities. To implement the validation plan, new instrumentation and techniques have been developed and were briefly described in the text. The instrumentation required to carry out the plan exists or is in the final phase of testing. A data system for combining the validation data from the sources we have described with MODIS imagery is being developed at the University of Miami under the direction of R. Evans. We believe that the plan as described will provide a measure of the uncertainty expected to be associated with the atmospheric correction of MODIS. It will also provide data to allow "fine tuning" of the correction algorithm using MODIS data. If carried out, it should allow establishment of the correction uncertainty characteristic of oceanic regions for which atmospheric correction is normally expected to be excellent and provide an estimate of the increase in uncertainty in settings in which the correction is expected to be degraded.

Acknowledgments. The authors are grateful for support from the NASA Goddard Space Flight Center under contracts NAS5-31746 and NAS5-31734 (the SeaWiFS Project), NAS5-31363 and S-19864-E (the EOS/MODIS Project), and from the NASA Headquarters, Ocean Biology Program, under grant NAGW-273. In addition, we acknowledge the excellent support of the University of Hawaii Marine Operations Office and their provision of dockside space for the MOBY Operations site. Finally, we thank C. R. McClain and S. B. Hooker for providing a careful review resulting in significant improvements of the manuscript.

References

Asrar, G., and J. Dozier, *EOS: Science Strategy for the Earth Observing System*, 119 pp., Am. Inst. of Phys., Woodbury, N. Y., 1994.

Austin, R. W., The remote sensing of spectral radiance from below the ocean surface, in *Optical Aspects of Oceanography*, edited by N. G. Jerlov and E. S. Nielsen, pp. 317–344, Academic, San Diego, Calif., 1974.

Clark, D. K., E. T. Baker, and A. E. Strong, Upwelled spectral radiance distribution in relation to particulate matter in sea water, *Boundary Layer Meteorol.*, *18*, 287–298, 1980.

d'Almeida, G. A., R. Jaenicke, P. Roggendorf, and D. Richter, New sunphotometer for network operation, *Appl. Opt.*, *22*, 3796–3801, 1983.

Deschamps, P. Y., M. Herman, and D. Tanre, Modeling of the atmospheric effects and its application to the remote sensing of ocean color, *Appl. Opt.*, *22*, 3751–3758, 1983.

Frouin, R., M. Schwindling, and P. Y. Deschamps, Spectral reflectance of sea foam in the visible and near infrared: In situ measurements and implications for remote sensing of ocean color and aerosols, *J. Geophys. Res.*, *101*, 14,361–14,371, 1996.

Gao, B.-C., A. F. H. Goetz, and W. J. Wiscombe, Cirrus cloud detection from airborne imaging spectrometer data using the 1.38 micron water vapor band, *Geophys. Res. Lett.*, *20*, 301–304, 1993.

Gordon, H. R., Ship perturbation of irradiance measurements at Sea 1: Monte Carlo simulations, *Appl. Opt.*, *23*, 4172–4182, 1985.

Gordon, H. R., Remote sensing of ocean color: A methodology for dealing with broad spectral bands and significant out-of-band response, *Appl. Opt.*, *34*, 8363–8374, 1995.

Gordon, H. R., Atmospheric correction of ocean color imagery in the Earth Observing System era, *J. Geophys. Res.*, this issue.

Gordon, H. R., and D. K. Clark, Clear water radiances for atmospheric correction of coastal zone color scanner imagery, *Appl. Opt.*, *20*, 4175–4180, 1981.

Gordon, H. R., and K. Ding, Self-shading of in-water optical instruments, *Limnol. Oceanogr.*, *37*, 491–500, 1992.

Gordon, H. R., and M. Wang, Retrieval of water-leaving radiance and aerosol optical thickness over the oceans with SeaWiFS: A preliminary algorithm, *Appl. Opt.*, *33*, 443–452, 1994a.

Gordon, H. R., and M. Wang, Influence of oceanic whitecaps on atmospheric correction of SeaWiFS, *Appl. Opt.*, *33*, 7754–7763, 1994b.

Gordon, H. R., and T. Zhang, How well can radiance reflected from the ocean-atmosphere system be predicted from measurements at the sea surface?, *Appl. Opt.*, *35*, 6527–6543, 1996.

Gordon, H. R., D. K. Clark, J. L. Mueller, and W. A. Hovis, Phytoplankton pigments derived from the Nimbus-7 CZCS: Initial comparisons with surface measurements, *Science*, *210*, 63–66, 1980.

Gordon, H. R., O. B. Brown, R. H. Evans, J. W. Brown, R. C. Smith, K. S. Baker, and D. K. Clark, A semianalytic radiance model of ocean color, *J. Geophys. Res.*, *93*, 10,909–10,924, 1988.

Gordon, H. R., T. Zhang, F. He, and K. Ding, Effects of stratospheric aerosols and thin cirrus clouds on atmospheric correction of ocean color imagery: Simulations, *Appl. Opt.*, *36*, 682–697, 1997.

Holben, B. N., et al., Automatic Sun and sky scanning radiometer system for Network Aerosol Monitoring, *Remote Sens. Environ.*, in press, 1997.

Johnson, B. C., S. S. Bruce, E. A. Early, J. M. Houston, T. R. O'Brian, A. Thompson, S. B. Hooker, and J. L. Mueller, *The Fourth SeaWiFS Intercalibration Round-Robin Experiment, SIRREX-4, May 1995*, *SeaWiFS Tech. Rep. Ser.*, *vol. 37*, *NASA Tech. Memor. 104566*, 1996.

Kaufman, Y. J., A. Gitelson, A. Karnieli, E. Ganor, R. S. Fraser, T. Nakajima, S. Mattoo, and B. N. Holben, Size distribution and scattering phase functions of aerosol particles retrieved from sky brightness measurements, *J. Geophys. Res.*, *99*, 10,341–10,356, 1994.

King, M. D., and B. M. Herman, Determination of the ground albedo and the index of absorption of atmospheric particulates by remote sensing, I, Theory, *J. Atmos. Sci.*, *36*, 163–173, 1979.

King, M. D., D. M. Byrne, B. M. Herman, and J. A. Reagan, Aerosol size distributions obtained by inversion of optical depth measurements, *J. Atmos. Sci.*, *35*, 2153–2167, 1978.

Klenk, K. F., P. K. Bhartia, E. Hilsenrath, and A. J. Fleig, Standard ozone profiles from balloon and satellite data sets, *J. Clim. Appl. Meteorol.*, *22*, 2012–2022, 1983.

Koepke, P., Effective Reflectance of oceanic whitecaps, *Appl. Opt.*, *23*, 1816–1824, 1984.

Liu, Y., Measurement of the intensity and polarization of light in the atmosphere, Ph.D. dissertation, 171 pp., Univ. of Miami, Coral Gables, Fla., 1996.

Moore, K. D., K. J. Voss, and H. R. Gordon, Measurements of the spectral reflectance of whitecaps in the open ocean, *Eos Trans. AGU*, *76*, OS105, 1996.

Morel, A., and B. Gentili, Diffuse reflectance of oceanic waters: Its dependence on Sun angle as influenced by the molecular scattering contribution, *Appl. Opt.*, *30*, 4427–4438, 1991.

Morel, A., and B. Gentili, Diffuse reflectance of oceanic waters, II, Bidirectional aspects, *Appl. Opt.*, *32*, 6864–6879, 1993.

Morel, A., K. J. Voss, and B. Gentili, Bidirectional reflectance of oceanic waters: A comparison of modeled and measured upward radiance fields, *J. Geophys. Res.*, *100*, 13,143–13,150, 1995.

Mueller, J. L., *The First SeaWiFS Intercalibration Round-Robin Experiment, SIRREX-1, July 1992, SeaWiFS Tech. Rep. Ser., Vol. 14, NASA Tech. Memor. 104566*, 1993.

Mueller, J. L., and R. W. Austin, *Ocean Optics Protocols for SeaWiFS Validation, SeaWiFS Tech. Rep. Ser., Vol. 5, NASA Tech. Memor. 104566*, 1992.

Mueller, J. L., and R. W. Austin, *Ocean Optics Protocols for SeaWiFS Validation, Revision 1, SeaWiFS Technical Report Series: Vol. 25, NASA Tech. Memor. 104566*, 1995.

Mueller, J. L., B. C. Johnson, C. L. Cromer, J. W. Cooper, J. T. McLean, S. B. Hooker, and T. L. Westphal, *The Second SeaWiFS Intercalibration Round-Robin Experiment, SIRREX-2, June 1993, SeaWiFS Tech. Rep. Ser., Vol. 16, NASA Tech. Memor. 104566*, May 1994.

Mueller, J. L., B. C. Johnson, C. L. Cromer, S. B. Hooker, J. T. McLean, and S. F. Biggar, *The Third SeaWiFS Intercalibration Round-Robin Experiment, SIRREX-3, September 1994, SeaWiFS Tech. Rep. Ser., Vol. 34, NASA Tech. Memor. 104566*, 1996.

Nakajima, T., M. Tanaka, and T. Yamauchi, Retrieval of the optical properties of aerosols from aureole and extinction data, *Appl. Opt.*, *22*, 2951–2959, 1983.

Nicolet, M., The solar spectral irradiance and its action in the atmospheric photodissociation processes, *Planet. Space Sci.*, *29*, 951–974, 1981.

Salomonson, V. V., W. L. Barnes, P. W. Maymon, H. E. Montgomery, and H. Ostrow, MODIS: Advanced facility instrument for studies of the Earth as a system, *IEEE Geosci. Remote Sens.*, *27*, 145–152, 1989.

Sasano, Y., and E. V. Browell, Light scattering characteristics of various aerosol types derived from multiple wavelength lidar observations, *Appl. Opt.*, *28*, 1670–1679, 1989.

Schwindling, M., Modeles et measures pour l'observation spatiale de la couleur de l'ocean: Diffusion atmospherique par les aerosols et reflexion de surface par l'ecume, 1995, Doct. de l'Univ. thèse, 245 pp., Univ. des Sci. et Technol. de Lille, Lille, France, 1995.

Shettle, E. P., and R. W. Fenn, Models for the aerosols of the lower atmosphere and the effects of humidity variations on their optical properties, *AFGL-TR-79-0214*, Air Force Geophys. Lab., Hanscomb Air Force Base, Mass., 1979.

Spinhirne, J. D., Micro pulse lidar, *IEEE Trans. Geosci. Remote Sens.*, *31*, 48–55, 1993.

Vigroux, E., Contribution a l'étude experimentale de l'absorption de l'ozone, *Ann. Phys.*, *8*, 709–762, 1953.

Voss, K. J., Electro-optic camera system for measurement of the underwater radiance distribution, *Opt. Eng.*, *28*, 241–247, 1989.

Voss, K. J., and A. C. Chapin, Next generation in-water radiance distribution camera system, *Soc. Photo-Opt. Instrum. Eng.*, *1750*, 384–387, 1992.

Voss, K. J., and G. Zibordi, Radiometric and geometric calibration of a visible spectral electrooptic "fisheye" camera radiance distribution system, *J. Atmos. Oceanic Technol.*, *6*, 652–662, 1989.

Wang, M., and H. R. Gordon, Retrieval of the columnar aerosol phase function and single scattering albedo from sky radiance over the ocean: Simulations, *Appl. Opt.*, *32*, 4598–4609, 1993.

Young, A. T., Revised depolarization corrections for atmospheric extinction, *Appl. Opt.*, *19*, 3427–3428, 1980.

W. Broenkow, Moss Landing Marine Laboratories, San Jose State University, Moss Landing, CA 95039.

D. K. Clark, NOAA/NESDIS, Camp Springs, MD 20746.

Y. Ge, Research and Data Corporation, Greenbelt, MD 20770.

H. R. Gordon and K. J. Voss, Department of Physics, University of Miami, Coral Gables, FL 33124. (e-mail: gordon@phyvax.ir.miami.edu)

C. Trees, CHORS, San Diego State University, San Diego, CA 92120.

(Received May 9, 1996; revised October 1, 1996; accepted October 15, 1996.)